Towed Streamer EM data from Barents Sea, Norway

Anwar Bhuiyan, Eivind Vesterås and Allan McKay, PGS*

Summary

The measured Towed Streamer EM data from a survey in the Barents Sea, undertaken in the Norwegian sector are inverted as a series of unconstrained 2.5D inversion. We show that unconstrained anisotropic 2.5D inversion of the EM data in complex geological settings can produce resistivity models that are consistent with both interpreted log and seismic data, and known discoveries. We consider three cases from the surveys acquired over Skrugard, Caurus and Norvarg areas of Barents Sea. We have compared the results of unconstrained inversion to publically available log data at Skrugard discovery. Not only is the overall depth trend recovered, but the main variation of the resistivity is captured as well as, in some intervals, comparable average interval resistivity. We also show example resistivity and apparent anisotropy sections, while the resistivity section highlights that the sub-surface resistivity is complex, the somewhat simpler anisotropy section reveals an anisotropy anomaly that is co-incident with both the lateral, and depth, extent of Skrugard. The apparent anisotropy corresponds fairly well with Caurus and Norvarg anomalies. However, finding structural outline from the vertical resistivity alone is challenging by unconstrained inversion.

Introduction

As part of a larger acquisition campaign in 2013 we acquired high quality CSEM data, using a Towed Streamer EM system, in the Barents Sea; see Figure 1 for location and coverage of the acquisition. The areas are relatively under-explored, but a working hydrocarbon system is proven, encompass complex geological settings with relatively high and variable background resistivity throughout the sub-surface, and anisotropic sediments. In an exploration setting in areas with a complex geology it is important to be able to interpret the sub-surface resistivity with confidence. We present three brief case studies to show that it is possible to recover resistivity depth trends, the average interval resistivity, and interpretable resistivity sections, using unconstrained inversion of the acquired data.

Firstly, we show a comparison of the results of unconstrained 2.5D finite element inversion to publically available well-log data at the Skrugard discovery in the Barents Sea. We also consider an example resistivity and apparent anisotropy sections (ratio of vertical to horizontal resistivity) over the discovery.

2D dual sensor seismic data acquired over Skrugard in 2011 and 3D Mega-survey seismic data over Caurus were utilized to delineate subsurface structures, and to compare inverted resistivities (Figures 5 and 6).

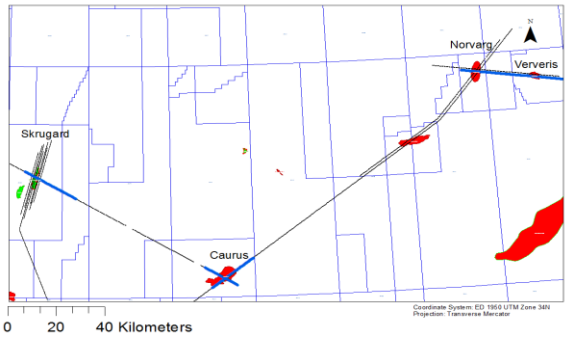

Figure 1: Location of data presented in this paper in blue, overlaid on full coverage in black.

Towed Streamer EM data

Towed streamer EM data were acquired utilizing a bi-pole source (800m long) towed at 10m below sea level and streamer based EM sensors towed simultaneously at a nominal depth of 100m. The source-signal sequence is 120s long with the active (runs at 1500 amperes) 90s followed by 30s no signal (used for background noise estimation in processing). The EM streamer has effectively 72 offsets varying from 50 – 7,800m. The towing speed was 4–5 knots.

The processing consists of de-convolving the measured electric field with the output source current to obtain the frequency responses for all available offsets, frequencies and shot points, and application of noise reduction algorithms (Mattsson et al., 2012). In this study we used data at the frequency range of 0.2-2.0 Hz.

Processed data along a survey line over Skrugard are shown as an example in Figure 2. The data are presented as the amplitude and phase over a selection of offsets (1943-6000m) and frequencies of 0.2 and 0.4 Hz. The data quality is good with stable amplitude and phase estimates over a broad frequency and offset range (overall total uncertainties of the data are <3%). The largest uncertainty is associated with the lowest frequency and the furthest offsets (Mattson et al., 2012).

DOI http://dx.doi.org/10.1190/segam2014-1202.1

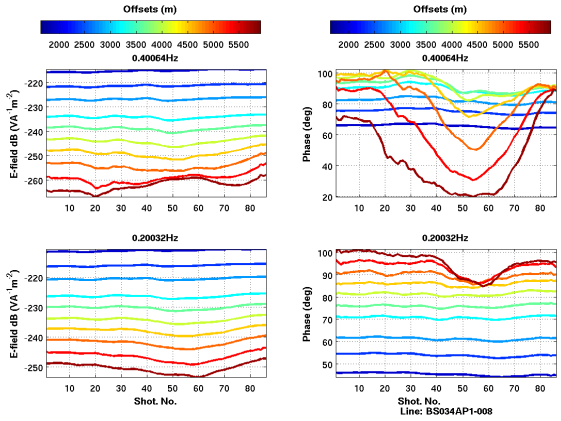

Figure 2: Subset of frequency response amplitudes (left panels) and phases (right panels) for a broad range of offsets. The shot number is a proxy for position along the survey line: each position is separated by about 250m.

Inversion Methodology & Performance

We used regularised unconstrained anisotropic 2.5D inversion to recover the sub-surface resistivity. The inversion code we used was the MARE2DEM code that is available via the Scripps Seafloor Electromagnetic Consortium. The forward modelling kernel of MARE2DEM is based on the adaptive finite element code of Key and Ovall (2011); the inversion scheme is based on smooth "Occam" inversion (Constable et al., 1987) with an additional anisotropy penalty.

The only fixed parameters in the inversion are the water resistivity and water depth. The water depth was fixed on the basis of the measured echo-sounder data, while the water resistivity was fixed by using daily measurements of the sea-water conductivity. 1D inversion was used to check that the water resistivity could be recovered by inversion and did not vary between measurement points. However, we have found that examining the inversion residuals from 2.5D inversion is an effective way of ensuring that the effective water resistivity chosen. In any case the chosen water resistivity is close to the average of the measured values.

For a given model parameterisation two main factors increase the computational burden of the inversion. Firstly, the bi-pole source and receivers, and geometry (e.g. orientations), is incorporated in the forward modelling kernel of the inversion. Secondly, the electric field is sampled densely in space (a source-point every ~250m), and the acquisition geometry means that employing reciprocity does not reduce the problem. Nevertheless, for a typical data selection and model parameterisation, consisting of about 10k data points and 20k model parameters, an inversion iteration takes about 25 minutes when 384 cores are employed. About 10-20 inversion iterations are usually sufficient to reach the pre-scribed target misfit.

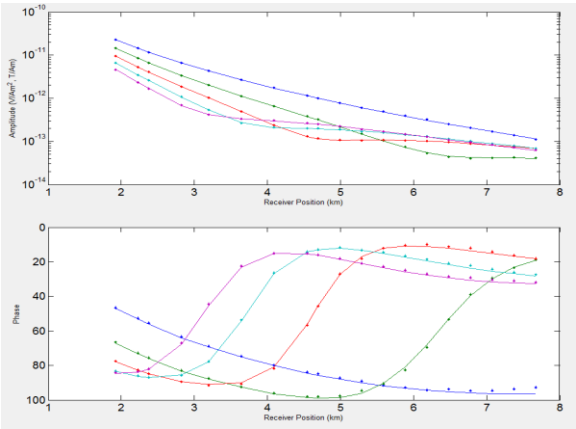

Figure 3: Data-fit, Caurus example. Dots are data-points and solid line is model-fit, there are uncertainty bars on the data-points but they are hard to see on this scale.

The first pass inversion data selection and parameterisation for the Barents Sea data sets were refined with optimized water conductivity, frequency/offset selection and dense-grid initial model input. The results we show here are based on selection of the five lowest frequencies (0.2:0.2:1 Hz), and 19 offsets in the range 1.9 to 7.8 km. Here, we show an example of data-fit (Figure 3) for the parameterization implemented in Barents Sea EM data inversion, which provide residual misfit less than 3%. We continue to test the optimum data selection and model parameterization as part of the inversion appraisal workflow (the results of which are not shown here).

Well Log Comparison

We have compared the inverted resistivity to the publically available well-log data in the Barents Sea area. For example, Figure 4 shows the resistivity log (horizontal resistivity) from the well (7222/8-1) at Skrugard, and the pseudo-well logs extracted from the unconstrained inversion of a nearby survey profile.

The overall resistivity trend observed in the well-log has been recovered fairly well in the inverted data. A high resistivity anomaly has been recovered at depths of 1250–1450m below sea level which corresponds to the Skrugard discovery (Løseth et al., 2013). We think our results indicate that it may be possible to get closer to the intrinsic resolution of CSEM data, without resorting to constrained inversion, given precise (Myer et al., 2012), densely sampled data, and a finely parameterised unconstrained inversion domain.

DOI http://dx.doi.org/10.1190/segam2014-1202.1

A reasonable data-fit between inverted and well-log resistivities has been observed at the reservoir (vertical resistivity) and in the under burden. The inverted resistivity in the overburden is higher compared to well-log data (Figure 4). However the tri-axial well-log published by Løseth et al., (2013) and Nguyen et al., (2013), shows higher vertical resistivity (4-5 Ωm) at the overburden which corresponds well with our results. In addition anisotropy is penalised in the same way as roughness preferring a more isotropic solution if possible. We're currently investigating the behaviour when relaxing this parameter.

Inverted horizontal resistivity at the reservoir is low compared to the log data, since the electric field mode is mainly vertical within a thin resistive layer (Løseth and Ursin, 2007). Therefore, a significant variation between the vertical and horizontal resistivity has been recovered at the reservoir level (Figure 4). We exploit the apparent electrical anisotropy (the ratio of the vertical to horizontal resistivity) in detecting high-resistivity layer in the next section.

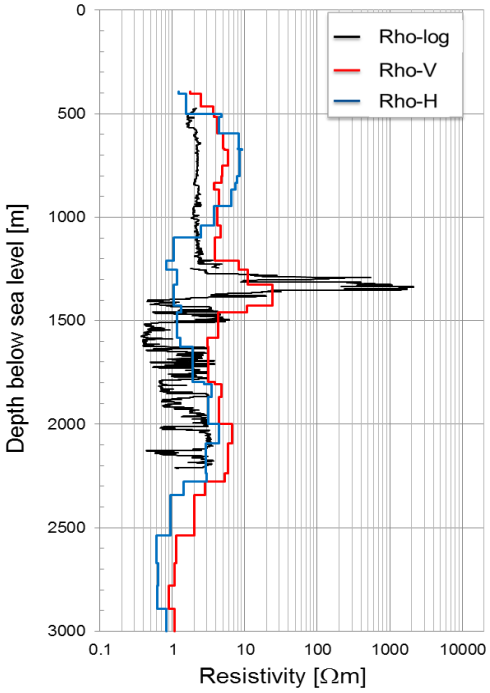

Figure 4: Example comparison between the measured resistivity at one well in the Barents Sea and the resistivity recovered via anisotropic inversion.

Sub-Surface Resistivity in the Barents Sea

We have inverted all 8 lines of Towed Streamer EM data in the vicinity of Skrugard, the discovery of which was a major milestone in the exploration of the Barents Sea. The average relative misfit in most cases is less than about 3%.

In Figure 5 we show an example result from the inversion in terms of the vertical resistivity, and the apparent anisotropy. The line shown in the upper panel crosses the short axis of Skrugard (about 2km wide) over the surface location of the 7222/5-1 appraisal well completed in 2012. It is approximately perpendicular to the geological strike direction of the structure. The resistivity sections have been co-rendered with depth stretched (using the velocities from seismic processing) stacked seismic data. The seismic data are from a previous survey in 2011, and the seismic line is about 1km south of the EM line shown.

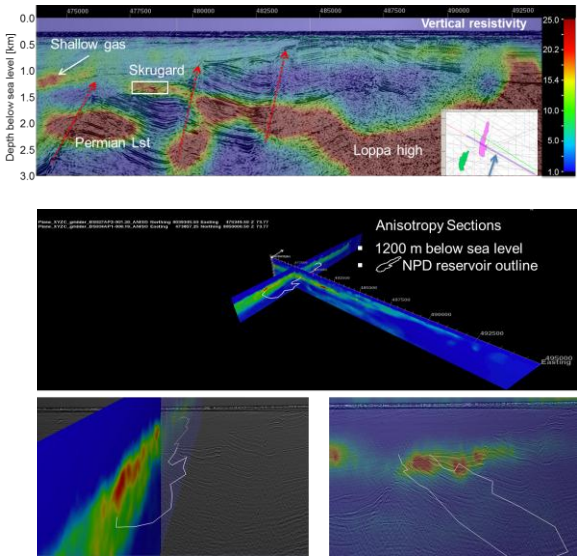

Figure 5: The vertical resistivity (Ωm) (top) and apparent anisotropy (middle) sections in the Skrugard area overlain on the dual sensor seismic data. The inset map (top) shows the relative position of the EM and seismic data shown here. The white box shows the approximate location of Skrugard. The lower sections show the extent of apparent anisotropy along a strike-line (left) and cross-line (right) with respect to regional strike of the structure. Structural outline is shown by white polygon.

The vertical resistivity suggests quite a complex resistivity structure in the vicinity of Skrugard. However, the apparent anisotropy indicates that the vertical and horizontal (not shown for brevity) sub-surface resistivity co-vary in space, but there are obvious apparent anisotropy anomalies. The strongest apparent anisotropy is restricted to the precise lateral location of Skrugard, and is remarkably well registered in depth given that we have used unconstrained inversion. At the appraisal well location, the top Skrugard reservoir level is 1276 m below mean sea level; the Oil Water Contact is at 1395m. The apparent anisotropy anomaly is between 1200 and 1500 m.

The 2D assumption in the inversion scheme works better perpendicular to the strike-line than along the strike line, resulting in better depth resolution on the line across

DOI http://dx.doi.org/10.1190/segam2014-1202.1

Skrugard (Figure 5). There are two additional apparent anisotropy anomalies: the anisotropy anomaly to the west of Skrugard is most likely due to shallow gas and the origin of the anomaly east to Skrugard is unknown. The possible gas leakage paths through the deep-routed faults (red stippled arrows, Figure 5) cause primary and/or secondary migration of HC generated from deeply buried source rocks.

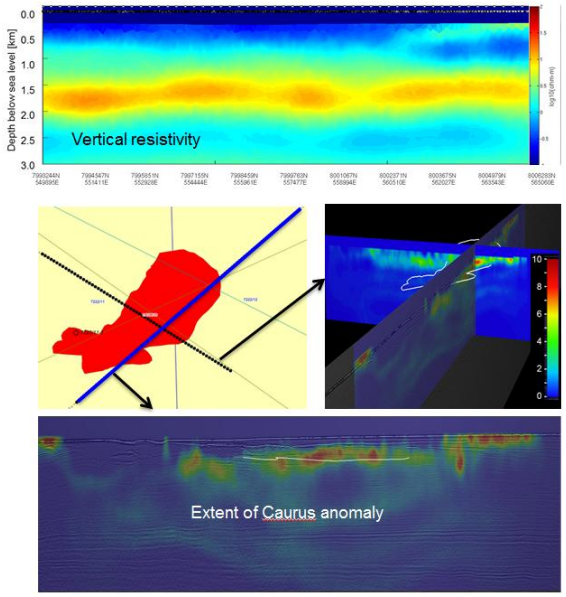

Figure 6: The vertical resistivity (Ωm) (top) and apparent anisotropy (bottom) section in the Caurus area. The middle-right panel shows apparent anisotropy sections along the EM lines running along and across the strike of the Caurus structure.

In Figure 6 we show an example result from the inversion in terms of the vertical resistivity, and apparent anisotropy along the EM lines running along and across the strike of the Caurus structure. The anisotropy section along the strike-line has been co-rendered with depth stretched seismic data.

Inverted vertical resistivity suggests a deep regional resistivity distribution with shallow inhomogeneity. It is difficult to differentiate the Caurus anomaly since the resistivity contrast of the reservoir is weak with respect to background (Well 7222/11-1, not shown). However, the apparent anisotropy indicates a strong anomaly restricted to the lateral extent and depth of Caurus (750-800m below sea level). The apparent anisotropy anomaly to the south of Caurus is most likely due to shallow inhomogeneity while the origin of the anomaly to north is unknown.

Finally, in Figure 7 we show an example result along the EM line running over Norvarg and Ververis (Figure 1). Seismic and well log (not shown for brevity) data indicate a multi-layer structure and low resistivity contrast with respect to the background. It is, therefore, difficult to differentiate the Norvarg anomaly in the inverted vertical resistivity section. However, the apparent anisotropy indicates a strong anomaly restricted to the lateral extent of Norvarg structure and registered in shallow depth (800-950m below sea level, Figure 7). The origin of the shallow anomaly east to Norvarg is unknown. The resistivity contrast for Ververis might be too small to be detected in this level of unconstrained inversion.

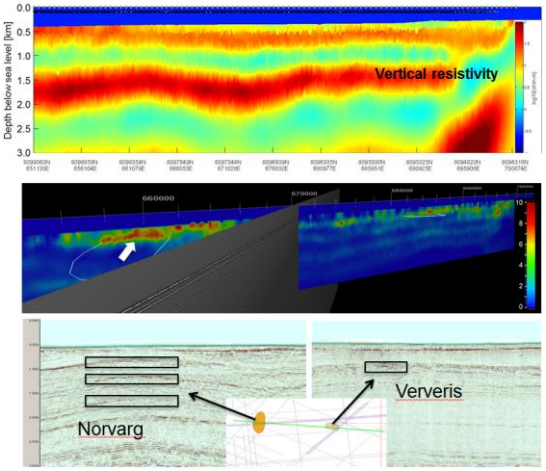

Figure 7: The vertical resistivity (Ωm) (top) and apparent anisotropy (middle) section in the Norvarg area. Lower panels show the Norvarg and Ververis structures.

Summary & Conclusions

Unconstrained anisotropic 2.5D inversion of Towed Streamer EM data from Barents Sea produces resistivity models that are consistent with interpreted well log and seismic data, at known discoveries in the case of Skrugard. We think our results indicate that it may be possible to get closer to the intrinsic resolution of CSEM data, without resorting to constrained inversion, given precise densely sampled data, and a well parameterised unconstrained inversion domain. The time spent on unconstrained inversion can produce "fast-track" results that are robust and interpretable. In addition it provides valuable input for parameters and constraints in a structurally constrained inversion. A 3D inversion of the EM data over Skrugard and constrained inversions for Caurus and Norvarg area remain further investigation for a precise subsurface interpretation.

Acknowledgements

We thank Petroleum-Geo Services (PGS) for permission to publish this work.

DOI http://dx.doi.org/10.1190/segam2014-1202.1

http://dx.doi.org/10.1190/segam2014-1202.1

EDITED REFERENCES

Note: This reference list is a copy-edited version of the reference list submitted by the author. Reference lists for the 2014 SEG Technical Program Expanded Abstracts have been copy edited so that references provided with the online metadata for each paper will achieve a high degree of linking to cited sources that appear on the Web.

REFERENCES

Constable, S. C., R. L. Parker, and C. G. Constable, 1987, Occam's inversion: A practical algorithm for generating smooth models from electromagnetic sounding data: Geophysics, **52**, 289–300, http://dx.doi.org/10.1190/1.1442303.

Key, K., and J. Ovall, 2011, A parallel goal-oriented adaptive finite element method for 2.5D electromagnetic modeling: Geophysical Journal International, **186**, no. 1, 137–154, http://dx.doi.org/10.1111/j.1365-246X.2011.05025.x.

Løseth, L. O., and B. Ursin, 2007, Electromagnetic fields in planarly layered anisotropic media: Geophysical Journal International, **170**, no. 1, 44–80, http://dx.doi.org/10.1111/j.1365-246X.2007.03390.x.

Løseth, L. O., T. Wiik, P. A. Olsen, A. Becht, and J. O. Hansen, 2013, CSEM exploration in the Barents Sea, Part I — Detecting Skrugard from CSEM: Presented at the 75th Annual International Conference and Exhibition, EAGE.

Mattsson, J., P. Lindqvist, R. Juhasz, and E. Björnemo, 2012, Noise reduction and error analysis for a towed EM System: 82nd Annual International Meeting, SEG, Expanded Abstracts, doi: 10.1190/segam2012-0439.1.

Myer, D., S. Constable, and K. Key, 2012, CSEM uncertainties and inversion: Presented at the 82nd Annual International Meeting, SEG.

Nguyen, A. K., Ø. Kjøsnes, and J. O. Hansen, 2013, CSEM exploration in the Barents Sea, Part II — High-resolution CSEM inversion: Presented at the 75th Annual International Conference and Exhibition, EAGE.